IEEE Access
Multidisciplinary | Rapid Review | Open Access Journal

Received December 13, 2020, accepted January 13, 2021, date of publication January 18, 2021, date of current version January 26, 2021.

Digital Object Identifier 10.1109/ACCESS.2021.3052535

Passive Positioning of Flying Object With Microwave Signals From LEO Satellites: Concept and Preliminary Simulation Results

DEFENG DAVID HUANG, (Senior Member, IEEE)
Department of Electrical, Electronic and Computer Engineering, The University of Western Australia, Perth, WA 6009, Australia
e-mail: david.huang@uwa.edu.au

This work was supported in part by the Australian Research Council Discovery Project under Grant DP190100786.

ABSTRACT Along with the deployment of low earth orbit (LEO) satellite constellations for global Internet services, Ku, Ka or V band microwave signals will be available from space anywhere on Earth. Utilizing the signals, a new approach to positioning flying objects passively is proposed, and a diffraction model to characterize the impact of the flying object on the intensity of the received signals is presented. A linear Minimum Mean Squared Error (MMSE) based estimator is then employed to position the flying object passively. Preliminary 2D simulation results are used to validate the effectiveness of the proposed method.

INDEX TERMS Low earth orbit satellites, microwave propagation, passive microwave remote sensing.

I. INTRODUCTION

Over the past decade, device-free passive (DfP) localizations [1], with which the tracked identity need neither carry devices nor participate actively in the localization algorithm, have been extensively investigated to sense human activities, by utilizing the fact that human activities impact the propagation of radio signals in particular the WiFi signals [1]–[3]. Like the DfP localizations, in this paper, a new approach to the detection of flying objects in the sky with the microwave signals from satellites in space, specifically the Low Earth Orbit (LEO) satellites, is proposed.

Today there are more than two thousand active satellites in space. Along with the deployment of LEO satellite constellations for global Internet services, there will be many more to come. For example, on 25 November 2020, SpaceX launched its fifteenth batch of 60 ''operational'' satellites for its Starlink constellation [4]. All the LEO satellite constellations for global Internet services use the high Ku, Ka, and/or V microwave frequency bands for digital communications, due to the availability of large channel bandwidth in those frequency bands. Like DfP localizations leveraging on the WiFi technology, when the global LEO based satellite Internet services are available commercially, the cost to build and deploy the ground receivers will be very low, due to economies of scale.

The associate editor coordinating the review of this manuscript and approving it for publication was Mohammad Tariqul Islam.

On the other hand, unmanned aerial vehicles (UAVs, also known as drones) have found fast-growing applications, thereby there are more and more flying objects in the sky, leading to the important problem of how to position and track them. To solve the problem, several methods have been available, including those based on radar, acoustic receivers, visible/infra-red camera, and RF sensing [5]–[10]. While those methods can solve the problem for some specific application scenarios, finding cost-effective solutions with high resolution and high availability is still a challenge, particularly for the important application scenario that the flying objects are un-cooperative. As an example, a lot of resources have been used to search the missing Malaysia Airlines Flight M370, but to date without success [11].

The proposed method has a potential to become a high-resolution cost-effective solution to position and track flying objects. Two possible ways to use the method are envisioned. One is to use customized ground terminals to eavesdrop the microwave signals from the satellites, thereby each terminal can be treated as a passive sensor. The other is to adapt the existing satellite communication infrastructure, particularly the user terminals and/or the satellite gateways, to monitor and analyze the signal intensity of each communication channel, either downlink or uplink. In this paper, we are focused on the first to provide a preliminary feasibility study to the proposed method.

We first analyze the first Fresnel zone radius of a flying object, which demonstrates that a flying object about 1m and

10m in size will have a significant impact on Ku, Ka or V band signals, for a flight height about 100m and 1,000m, respectively. A diffraction model is then developed to investigate the time variation of the received signal intensity due to the obstruction of the flying object. By modeling the flying object as a rectangular slab, preliminary simulation results show that some attributes of the flying object, e.g. speed and size, relate to the time variation pattern of the received signals, thereby potentially those attributes of flying objects could be estimated by analyzing the intensity of the received signals. Particularly, it is found that the received signal varies significantly for up to about 0.2 second if the flying object crosses the baseline (i.e. the communication link between the satellite and the ground station).

Utilizing the time variation of the received signal intensity, a signal processing model regarding the location of the flying object is proposed, which enables us to develop a linear Minimum Mean Squared Error (MMSE) based estimator to passively estimate its location with received signals at multiple ground stations. Preliminary 2D simulation results show that high precision positioning could be achieved with a distance between adjacent ground stations as small as 50m - 200m, when five satellites are observable in the same time by the ground stations. For a large distance between adjacent ground stations, e.g. 1,600m, it is still possible to position the flying object, albeit with much reduced precision.

The idea of utilizing signals emitted from artificial satellites or stars to estimate things on Earth or space is not new. For example, stellar occultations were used to observe the atmosphere of planets [12]; using the L band microwave signals from satellites of Global Positioning Systems (GPS)/Global Navigation Satellite Systems (GNSS), the sea states and the soil moisture were monitored with the GNSS Reflectometry (GNSS-R) technology [13], and maps of atmospheric water vapor were made with GPS meteorology [14]; the GNSS Radio Occultation payload has been installed on dedicated LEO satellites (e.g. the COSMIC satellite constellation) and can also be installed on flexible 'Space-as-a-Service' platforms (e.g. Spire's Lemur satellites), due to its importance to weather forecasting; atmospheric variables beyond water vapor have been proposed to be monitored by the NASA and NSF funded Active Temperature, Ozone and Moisture Microwave Spectrometer (ATOMMS) program [15], [16] and the European Space Agency funded Normalized Differential Spectral Attenuation (NDSA) measurement technology [17]–[19]; recently, we have carried out research into 3D rainfall field retrieval with microwave signals from LEO satellites [20]–[23].

However, to the best of our knowledge, to date no one else has used the microwave signals from LEO satellite communication links to position and track flying objects in the atmosphere. Research on passive forward scatter radars with opportunistic satellite illuminators so far has been focused on using signals from geostationary orbit (GEO) satellites (e.g. DVB-S satellites) and medium earth orbit (MEO) satellites (e.g. GPS satellites)-unlike a LEO satellite, the GEO/MEO satellite can be treated as static during the short time that the flying object crosses the baseline; also it is reasonable to expect that in the future there will be many more LEO satellites available than GEO/MEO satellites. The only relevant work that explicitly mentioned LEO satellites is our very preliminary work on the diffraction effect of microwave signals by flying objects [24].

This paper is organized as follows. Sections II and III present the first Fresnel zone radius analysis and the proposed diffraction model, respectively. Section IV introduces a simple algorithm to passive positioning of a flying object with microwave signals received at multiple ground stations. Numerical results are presented in Section V, and conclusions are drawn in Section VI.

II. FRESNEL ZONE ANALYSIS

From diffraction theory, the microwave signal of a satellite communication system will be significantly obstructed when a flying object is near the line segment connecting the satellite and the ground receiver (as shown in Fig. 1),[1] if the size of the flying object is in the order of the first Fresnel zone radius F_1, which is approximately given by [25]

$$F_1 \approx \sqrt{\lambda d} \tag{1}$$

where λ is the wavelength of the microwave signal and d is the distance between the flying object and the ground receiver. Table 1 shows some examples of the first Fresnel zone radius for the Ku, Ka, and V band signals, which demonstrates that a flying object about 1m and 10m in size will have a significant impact on Ku/Ka/V band signals at a distance of 100m and 10,000m, respectively. Therefore, such a flying object may be detected by the ground receivers with microwave signals from satellites.

TABLE 1. First Fresnel zone radius F_1 for Ku, Ka, and V band microwave signals.

distance between flying object and ground receiver d (meter)	wavelength λ (centimetre)	first Fresnel zone radius F_1 (meter)
100	2.0 (Ku band, 15 GHz)	1.4
100	1.0 (Ka band, 30 GHz)	1.0
100	0.5 (V band, 60 GHz)	0.7
10, 000	2.0 (Ku band, 15 GHz)	14
10, 000	1.0 (Ka band, 30 GHz)	10
10, 000	0.5 (V band, 60 GHz)	7

III. DIFFRACTION MODEL

For the obstruction of microwave signals from a LEO satellite by a flying object as shown in Fig. 1, we propose a simplified diffraction model as shown in Fig. 2. Here the Cartesian coordinate is defined as follows. The origin of the coordinate is attached with the center of the flying object. The $x - y$ plane is perpendicular to the line segment that connects the

[1] In this paper, we are focused on signal transmission from LEO satellites to ground receivers. The analysis can also be applied to signal transmission from transmitters in ground stations to receivers on LEO satellites, due to the reciprocity of the transmission of microwave signals.

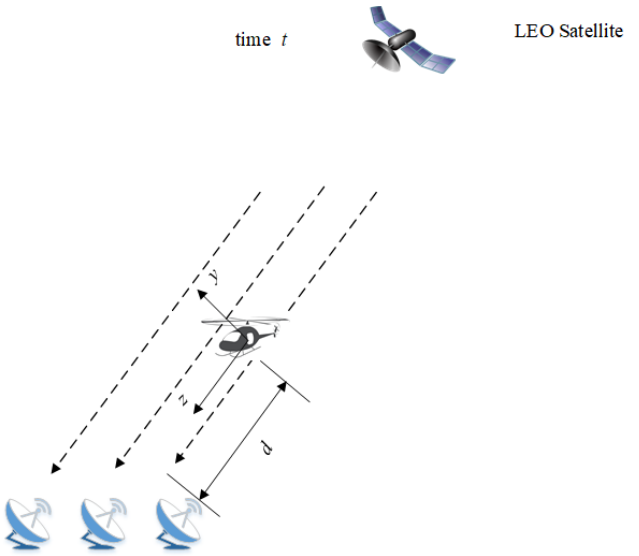

FIGURE 1. A simplistic geometric setup of a LEO satellite, a flying object and multiple ground receivers that are closely located. As the LEO satellite is far away, the communication links close to the ground stations can be approximately treated as parallel. The Cartesian coordinate is defined as follows. The origin of the coordinate is attached with the center of the flying object. The $x-y$ plane is perpendicular to the line segment between the satellite and ground stations, which is parallel to the z axis. x-coordinate is parallel with the ground, which is assumed flat.

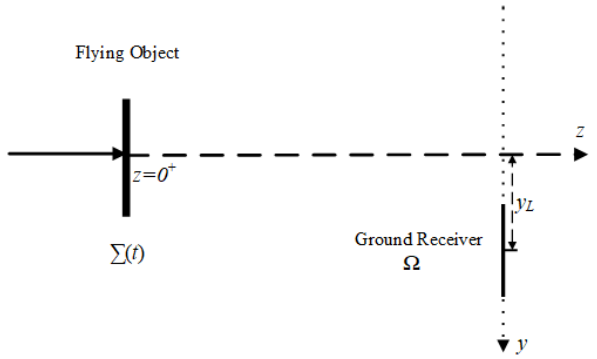

FIGURE 2. A diffraction model for a LEO satellite, a flying object and a receiver as shown in Fig. 1. As the satellite is far away, the waveform is approximately a plane wave. The Cartesian coordinate in this figure corresponds to that shown in Fig. 1.

satellite and the ground receiver of interest, which is parallel to the z axis. Applying Kirchhoff approximation [26], at time t, the complex amplitude of the microwave signal at plane $z = 0^+$ is then given by

$$T_{0^+}(x, y; t) = \begin{cases} 0, & \{x, y\} \in \Sigma(t) \\ B(t), & otherwise \end{cases}$$

where $B(t)$ is the complex amplitude of the incident wave if the flying object does not exist, and $\Sigma(t)$ is the 2D image of the flying object projected onto the $x-y$ plane.

Let $A_{0^+}(f_x, f_y; t)$ be the angular spectrum of the flying object at $z = 0^+$, which is the (spatial) Fourier transform of $T_{0^+}(x, y; t)$. The complex amplitude of the satellite signals at z is then given by [26]

$$U_z(x, y; t) = \frac{e^{jkz}}{j\lambda z} \int\int A_{0^+}(f_x, f_y; t) H_z(f_x, f_y) e^{j2\pi(f_x x + f_y y)} df_x df_y \tag{2}$$

where $H_z(f_x, f_y)$ is a given transfer function parametrized by z. Assume that the flying object is far away from the ground receiver, so the evanescent wave can be ignored. Then, at the ground receiver, the transfer function is given as follows [26].

$$H_z(f_x, f_y) = \begin{cases} e^{jz\sqrt{k^2 - 4\pi^2(f_x^2 + f_y^2)}}, & 4\pi^2(f_x^2 + f_y^2) < k^2 \\ 0, & otherwise \end{cases}$$

where the wave number $k = 2\pi/\lambda$.

If $(\alpha_x^2 + \alpha_y^2)_{max} \ll 1$, where $\alpha_x = \lambda f_x$ and $\alpha_y = \lambda f_y$ are the direction cosines in the x direction and the y direction, respectively, then

$$jz\sqrt{k^2 - 4\pi^2(f_x^2 + f_y^2)} \approx jkz\left(1 - \frac{\lambda^2(f_x^2 + f_y^2)}{2}\right).$$

Using the above approximation, the inverse Fourier transform of $H_z(f_x, f_y)$ can then be approximated by

$$h_z(x, y) \approx \frac{e^{jkz}}{\lambda z} e^{j\frac{\pi(x^2+y^2)}{\lambda z}}. \tag{3}$$

Using (3) and (2), we have the Fresnel approximation [26]:

$$U_z(x, y; t) \approx h_z(x, y) \otimes T_{0^+}(x, y; t) = \frac{e^{jkz}}{j\lambda z} \int\int T_{0^+}(x', y'; t) e^{j\frac{k((x-x')^2+(y-y')^2)}{2z}} dx' dy' \tag{4}$$

where $\otimes$ denotes linear convolution.

Furthermore, if the ground receiver is far away from the flying object (relative to its size), i.e. $k(x'^2 + y'^2)_{max} \ll z$, then from (4), we have the Fraunhofer approximation [26]:

$$U_z(x, y; t) \approx \frac{e^{jkz}}{j\lambda z} e^{j\frac{k(x^2+y^2)}{2z}} \int\int T(x', y', 0^+; t) e^{-j\frac{k(xx'+yy')}{z}} dx' dy'. \tag{5}$$

The intensity of the microwave signal is then given by

$$I_z(x, y; t) = |U_z(x, y; t)|^2 \tag{6}$$

Instead of using (2), (4) or (5) to compute the complex amplitude of the microwave signal, alternatively, we can first compute the complex amplitude of the microwave signal diffracted by a small hole that has exactly the same shape as the opaque 2D image $\Sigma(t)$, and then obtain the complex amplitude of the microwave signal diffracted by the 2D opaque image $\Sigma(t)$ using Babinet's principle.

A. EXAMPLE: A RECTANGULAR SLAB WITH NEGLIGIBLE HEIGHT

As the LEO satellite is far away, the microwave signal at the flight object can be approximately as a plane wave. Assume that the complex amplitude of the microwave signal $B(t)$ is a constant A. Let this plane wave go through a rectangular slab with width a (in the direction of x) and length b (in direction of y). Applying the Fraunhofer approximation and Babinet's principle, the complex amplitude at z is given by

$$\begin{aligned} U_z(x,y;t) &= A - Aab\frac{e^{jkz}}{j\lambda z}e^{j\frac{k(x^2+y^2)}{2z}}\frac{sin(\beta)}{\beta}\frac{sin(\gamma)}{\gamma} \\ &= A\left[1+\frac{jab}{\lambda z}e^{j\frac{k(x^2+y^2+2z^2)}{2z}}\frac{sin(\beta)}{\beta}\frac{sin(\gamma)}{\gamma}\right] \end{aligned}$$

where $\beta = \frac{\pi bx}{\lambda z}$ and $\gamma = \frac{\pi ay}{\lambda z}$.

The intensity of the signal is then given by

$$\begin{aligned} I_z(x,y;t) = A^2[1 &+ \frac{a^2b^2}{\lambda^2z^2}\frac{sin^2(\beta)}{\beta^2}\frac{sin^2(\gamma)}{\gamma^2} \\ &- \frac{2ab}{\lambda z}\frac{sin(\beta)}{\beta}\frac{sin(\gamma)}{\gamma}sin\frac{k(x^2+y^2+2z^2)}{2z}]. \end{aligned} \quad (7)$$

IV. A SIMPLE ALGORITHM FOR POSITIONING A FLYING OBJECT WITH MULTIPLE GROUND STATIONS

Assume that the effective aperture of the ground receiver antenna is Ω. The intensity measured by the ground receiver is then given by

$$G(t) = P_L\int\int_{\Omega} I_z(x,y;t)dxdy + w(t) \quad (8)$$

where $w(t)$ is the measurement noise, and $P_L = cd_{Sat}^2$ is the free space path loss (d_{Sat} is the distance between the LEO satellite and the ground station, c is a constant that is related to antenna gains and the carrier frequency of the communication system). For simplicity, we only consider the case that the communication system operates in the high signal to noise power ratio (SNR) region, thereby $w(t)$ is ignored in this paper.

For the ith satellite to the jth ground station, let $r_{i,j}(t)$ denote the measured received signal intensity in dB. Along with the movement of the LEO satellite, the impact of the free space path loss P_L can be removed by removing the linear trend in $r_{i,j}(t)$. After this removal, intuitively, the larger the variance $\sigma_{i,j}^2(t)$ of $r_{i,j}(t)$ in time, the more likely that the flying object crosses the baseline.

Assume that the coordinate[2] of the jth ground station is a three dimensional vector $g_j, j = 1, 2, \ldots, N_G$, where N_G is the number of ground stations, and that the coordinate of the ith satellite at time t is $\mathbf{s}_i(t), i = 1, 2, \ldots, N_S$, where N_S is the number of satellites. If the flying object is close to the line segment that connects satellite i and ground station j, then the coordinate of the flying object $\mathbf{x}(t)$ is assumed to be on the following line segment,

$$\mathbf{x}(t) = (1 - a_{i,j}(t))\hat{\mathbf{g}}_j(t) + a_{i,j}(t)\mathbf{s}_i(t) \quad (9)$$

where the real number $0 < a_{i,j}(t) < 1$ determines the location of the flying object on the line segment, and

$$\hat{\mathbf{g}}_j(t) = \mathbf{g}_j + \mathbf{n}_{i,j}(t) \quad (10)$$

where $\mathbf{n}_{i,j}(t)$ is a zero mean noise vector with its diagonal covariance matrix given by $\frac{1}{\sigma_{i,j}^2(t)}\mathbf{I}$ with $\mathbf{I}$ denoting an identity matrix.

By plugging (10) into (9), we have

$$\mathbf{x}(t) = \mathbf{g}_j + \mathbf{n}_{i,j}(t) - a_{i,j}(t)\left(\mathbf{g}_j - \mathbf{s}_i(t) + \mathbf{n}_{i,j}(t)\right) \quad (11)$$

for $i = 1, 2, \ldots, N_S$ and $j = 1, 2, \ldots, N_G$.

As the satellite is far away from the ground station, $\mathbf{g}_j - \mathbf{s}_i(t)$ are approximately the same for $1 \le j \le N_G$, i.e. those line segments are approximately parallel. Assume that the ground stations are not very close to each other. If there is only one flying object, then at any time given satellite i, there will be at most one ground station $\hat{j}(i)$ [3] with the microwave signals significantly impacted by the flying object, and

$$\hat{j}(i) = argmax_j\{\sigma_{i,j}^2\}.$$

As a result, $\sigma_{i,\hat{j}(i)}^2$ is relatively large, and $\mathbf{n}_{i,\hat{j}(i)}$ can be assumed to be small relative to $\mathbf{g}_j - \mathbf{s}_i$. Then (9) can be approximated by

$$\mathbf{x}(t) + a_{i,\hat{j}(i)}\left(\mathbf{g}_{\hat{j}(i)} - \mathbf{s}_i\right) = \mathbf{g}_{\hat{j}(i)} + \mathbf{n}_{i,\hat{j}(i)} \quad (12)$$

for $1 \le i \le N_S$.

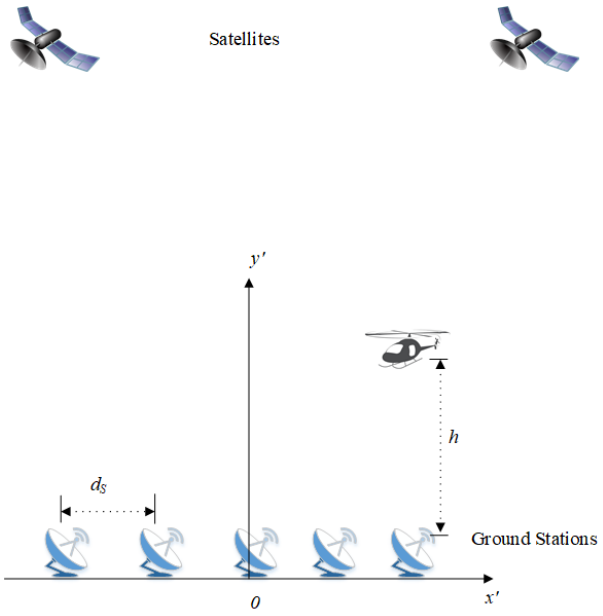

FIGURE 3. Relative positions among LEO satellites, flying object and ground stations.

[2]Note that the Cartesian coordinate here is different from that used to describe the diffraction model in Section III. Here the coordinate is stationary relative to the ground, as shown by the 2D coordinate $x' - y'$ in Fig. 3.

[3]From now on, the time index is dropped for the simplicity of presentation.

In matrix form, we have

$$\mathbf{Ab} = \mathbf{g} + \mathbf{n} \tag{13}$$

where

$$\mathbf{A} = \begin{bmatrix} I_3 & \mathbf{g}_{\hat{j}(1)} - \mathbf{s}_1 & 0 & \dots & 0 \\ I_3 & 0 & \mathbf{g}_{\hat{j}(2)} - \mathbf{s}_2 & \dots & 0 \\ \dots & \dots & \dots & \dots & \dots \\ I_3 & 0 & 0 & \dots & \mathbf{g}_{\hat{j}(N_S)} - \mathbf{s}_{N_S} \end{bmatrix}$$

$$\mathbf{b} = \begin{bmatrix} \mathbf{x} \\ a_{1,\hat{j}(1)} \\ a_{2,\hat{j}(2)} \\ \dots \\ a_{N_S,\hat{j}(N_S)} \end{bmatrix}$$

$$\mathbf{g} = \begin{bmatrix} \mathbf{g}_{\hat{j}(1)} \\ \mathbf{g}_{\hat{j}(2)} \\ \dots \\ \mathbf{g}_{\hat{j}(N_S)} \end{bmatrix}$$

$$\mathbf{n} = \begin{bmatrix} \mathbf{n}_{1,\hat{j}(1)} \\ \mathbf{n}_{2,\hat{j}(2)} \\ \dots \\ \mathbf{n}_{N_S,\hat{j}(N_S)} \end{bmatrix}$$

In this paper, we solve (13) using the following linear minimum mean squared error (MMSE) estimator:

$$\hat{\mathbf{b}} = \left(\mathbf{A}^{-1}\mathbf{V}_{\mathbf{n}}^{-1}\mathbf{A}\right)^{-1}\mathbf{A}^{-1}\mathbf{V}_{\mathbf{n}}^{-1}\mathbf{g} \tag{14}$$

where $\mathbf{V}_{\mathbf{n}}^{-1}$ is a diagonal matrix with its main diagonal given by $\sigma^2_{1,\hat{j}(1)}, \sigma^2_{1,\hat{j}(1)}, \sigma^2_{1,\hat{j}(1)}, \sigma^2_{2,\hat{j}(2)}, \dots, \sigma^2_{N_S,\hat{j}(N_S)}$. After $\hat{\mathbf{b}}$ is obtained, then the coordinate of the flying object is given by the first three elements of $\hat{\mathbf{b}}$. Using (14) to solve (13) means that the constraint $0 < a_{i,j} < 1$ is ignored. However, our empirical results in Section V-D demonstrate that the constraint is not material.

V. NUMERICAL RESULTS

A. SATELLITE ORBIT AND GROUND STATION LOCATIONS

We consider a circular LEO orbit with multiple satellites. The orbit height is assumed to be h_{Sat}. Therefore, the speed of the satellites is a constant. Earth's rotation is ignored. The ground stations are deployed on the the ground track of the satellites with equal distance d_S between adjacent ground stations, as shown in Fig. 3.

As shown in Fig. 4, the relationship between the elevation angle θ of a satellite relative to a ground station and the angle α relative to Earth center is as follows.

$$\theta = \frac{\pi}{2} - arctan\left(\frac{(h_{Sat} + r_E)sin(\alpha)}{(h_{Sat} + r_E)cos(\alpha) - r_E}\right) \tag{15}$$

where $r_E = 6.371 \times 10^6\ m$ is the radius of the Earth.

The distance between the satellite and the ground station d_{Sat} is then given by

$$d_{Sat} = \sqrt{(h_{Sat} + r_E)^2 - r_E^2 cos^2(\theta)} - r_E sin(\theta). \tag{16}$$

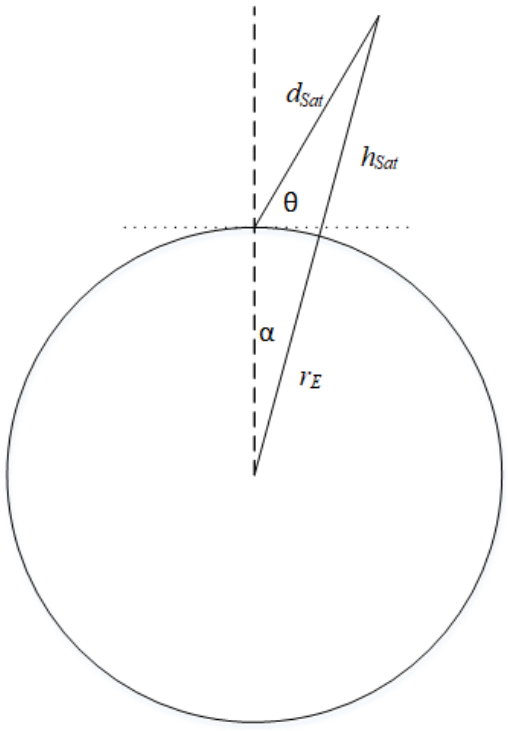

FIGURE 4. Relationship between θ, α and d_{Sat}.

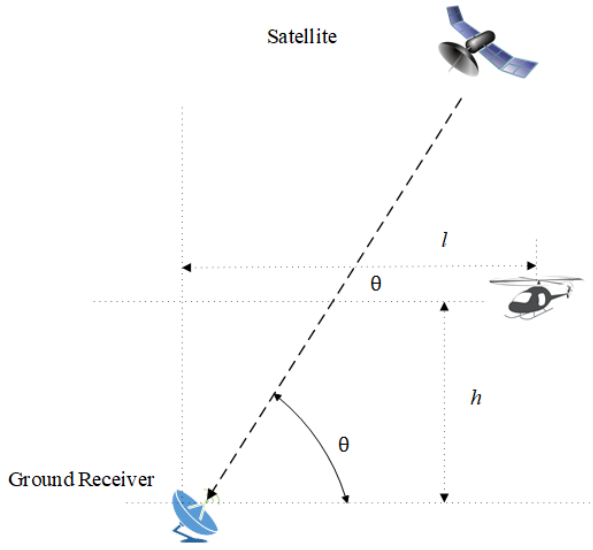

FIGURE 5. Relationship between θ, h and l for describing the relative positions between a ground receiver, a satellite and a flying object.

B. TRACK OF A FLYING OBJECT

Each ground station is equipped with multiple receivers with each receiver points to one LEO satellite. The flying object is approximated by a rectangular slab of width $a' = 10m$ (in the x direction) and length b'. The slab is always parallel with the ground, which is assumed to be flat. The intensity of the receiver is computed using (8) and (7). As shown in Figs. 3 and 5, the flying object flies above the ground

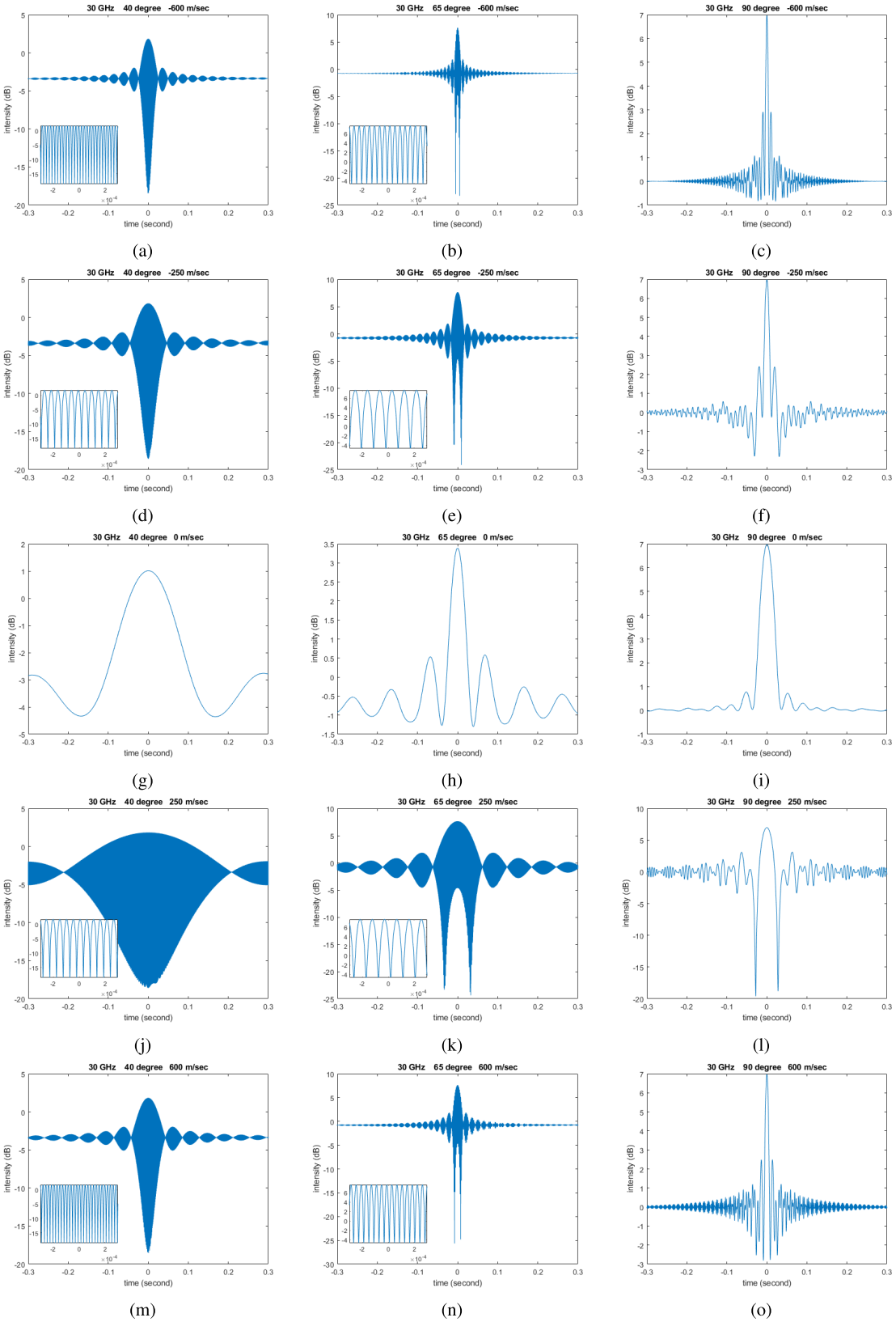

FIGURE 6. Time variation in intensity for a 30 GHz system with different elevation angles and different speeds of a flying object with $a' = 10m$ and $b' = 20m$. The time range for the subplots is $-3e{-}4$ to $3e{-}4$ second.

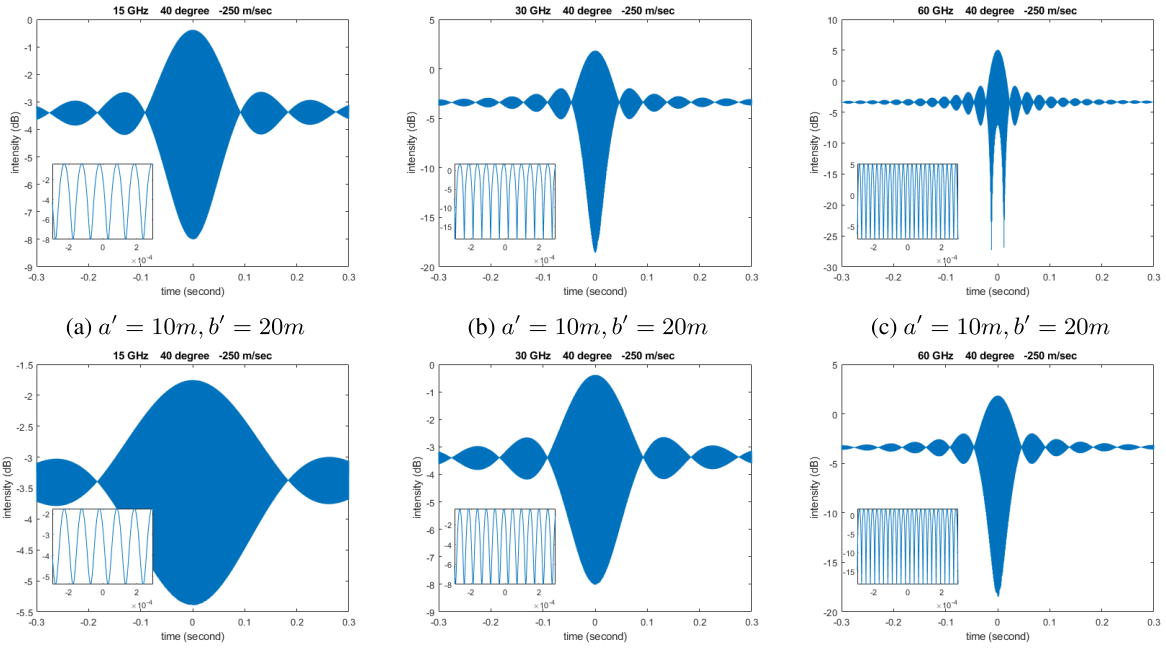

(a) $a' = 10m, b' = 20m$ (b) $a' = 10m, b' = 20m$ (c) $a' = 10m, b' = 20m$

(d) $a' = 10m, b' = 10m$ (e) $a' = 10m, b' = 10m$ (f) $a' = 10m, b' = 10m$

FIGURE 7. Time variation in intensity for 15 GHz, 30 GHz, 60 GHz systems with an elevation angle of 40° and a flying object speed of −250 m/s. The time range for the subplots is −3e−4 to 3e−4 second.

stations at a height of $h = 10,000m$ above the ground with a constant speed. The centroid of the flying object, if vertically projected onto the ground, is always on the ground track of the satellites. So only a 2D simulation is carried out.

Assume that the distance between the flying object and a reference line is l (see Fig. 5). When the satellite is at an elevation angle of θ, as shown in Fig. 5, the distance between the ground receiver and the centroid of the flying object projected onto the baseline is given by

$$z = \frac{h}{sin(\theta)} + \left[l - \frac{h}{tan(\theta)} \right] cos(\theta). \tag{17}$$

Also from Figs. 2 and 5, the distance between the centroid of the flying object and the baseline is given by

$$y_L = \left[l - \frac{h}{tan(\theta)} \right] sin(\theta). \tag{18}$$

From Figs. 2 and 5, it can be seen that, at an elevation angle of θ, the slab length in the direction of y axis is $b = b' sin(\theta)$, and in the direction of x axis is $a = a'$.

C. TIME VARIATION IN SIGNAL INTENSITY

The simulations are carried out as follows. For a LEO satellite of orbit height $h_{Sat} = 550km$, α is first generated, which changes at a speed of $\frac{2\pi}{T_{Sat}}$, where $T_{Sat} = 5,731.1$ seconds for $h_{Sat} = 550km$. Eqns. (15) and (16) are then used to obtain θ and d_{Sat}, respectively. The flying object is modeled by the rectangular slab as discussed in Section V-B. Eqns. (17), (18), (8) and (7) are used to compute the intensity of the received microwave signals. The ground receiver antenna is assumed to always point to the satellite of interest, and the aperture of the antenna (i.e. Ω in Eqn. (8)) is assumed to be $0.22m \times 0.22m$.

For a flying object modeled by a rectangular slab with $b' = 20m$, Fig. 6 shows the time variation of the received signal intensity for a 30 GHz system with a flight speed of -600m/s, -250m/s, 0m/s, 250m/s, and 600m/s and an elevation angle of 40°, 65° and 90°. A negative flight speed indicates that the flight object and the LEO satellites moves in the opposite direction. It can be seen that, except for an elevation angle at about 90^0 or a flight speed of about 0 m/s, the intensity of the received signals look like an amplitude modulated (AM) signal. Along with the increase of the speed of the flying object, the "carrier frequency" of the "AM" signal increases, and the width of the main lobe of the amplitude decreases. Compared with positive speed, the main lobe is narrower if the flying object is in negative speed. For all cases, there are significant variations in signal intensity for about 0.2 second, when the flying object crosses the baseline.

Fig. 7 shows the received signal intensity for 15 GHz, 30 GHz and 60 GHz systems with an elevation angle of 40° and a flight speed of −250 m/s. It can be seen that, when the system is increased from 15 GHz to 30 GHz and then to 60 GHz, the main lobe width of the envelope of the received signals decreases, and the "carrier frequency" of the "AM" signal increases. In terms of the variations in amplitude, the 60 GHz system varies more than the 30 GHz system, which varies more than the 15 GHz system. Also reducing b' from 20m to 10m increases the width of the main lobe, but decreases the degree of variation.

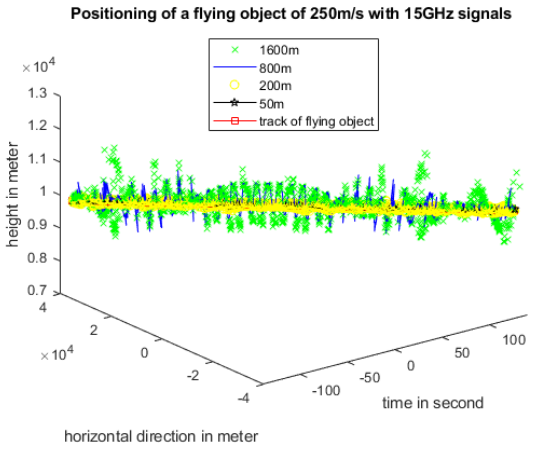

(a)

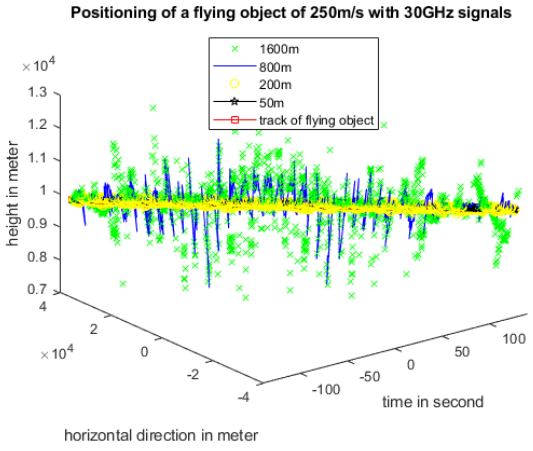

(b)

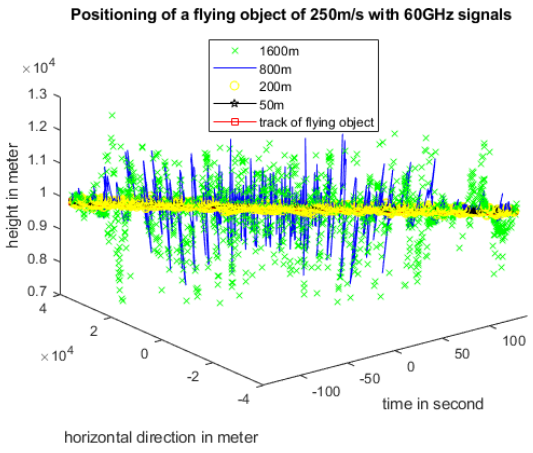

(c)

FIGURE 8. Positioning with different distances between adjacent ground stations (1,600m, 800m, 200m, 50m) using 5 satellites for a flying object with a speed of 250 m/s.

D. FLYING OBJECT POSITIONING WITH MULTIPLE GROUND STATIONS AND MULTIPLE LEO SATELLITES

The flying object is modeled by the rectangular slab as shown in Section V-C with $b' = 20m$. The speed of the flight object is assumed to be 250 m/s. Multiple LEO satellites and multiple ground stations are simulated. The difference in α between adjacent LEO satellites is set to be $\pi/180$ radian. Eqn. (14) is employed to retrieve the position of the flying object every 0.2 second. The variance of the noise vector in Eqn. (10) is computed using a window of 0.2 second.

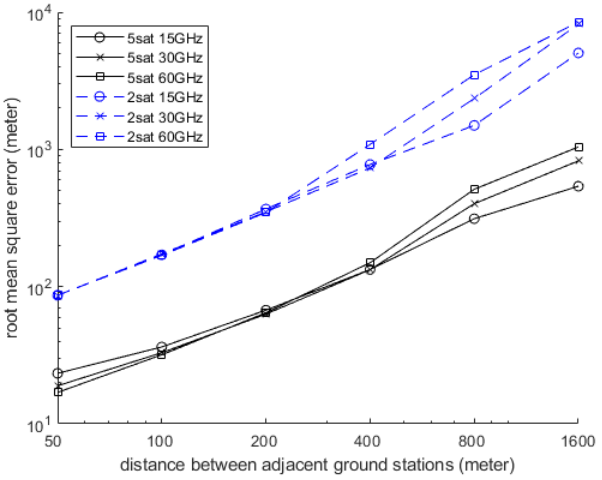

(a) MSE in horizontal direction

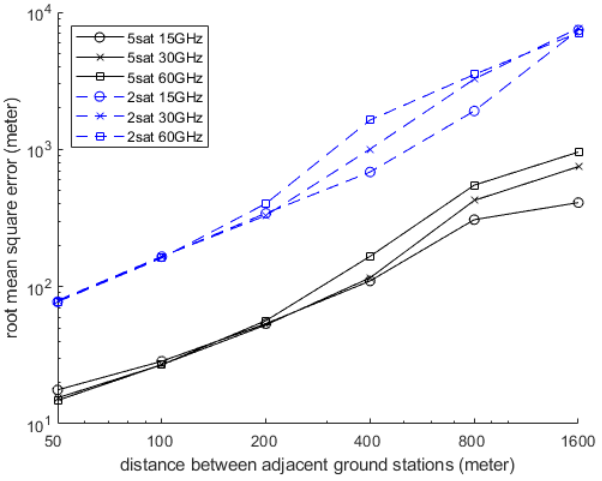

(b) MSE in height

FIGURE 9. Root Mean Squared Error for positioning a flying object with a speed of 250 m/s.

Fig. 8 shows the retrieved flying track in time using five satellites. It can be seen that when the distance between adjacent ground stations increases, the positioning precision decreases. However, even with a distance as large as 1,600m, it is still possible to detect the flying object, albeit with a low precision. To quantitatively characterize positioning performance, we define the root mean squared error as $\sqrt{\frac{1}{N}\sum_1^N(\hat{c}_i - c_i)^2}$, where $\hat{c}_i$ and c_i are the estimate and the true value, and N is the number of samples. Fig. 9 shows the root mean squared error performance of positioning in the horizontal direction and in height, for a system with two satellites and a system with five satellites. As expected, the system with five satellites is always better in root mean squared error performance than the system with two satellites. It can also be seen that for large distance (i.e. 400m, 800m

and 1,600m) between adjacent ground stations, the 15 GHz system is better than the 30 GHz system, which is better than the 60 GHz system. This is consistent with Fig. 8. However, when the distance is small (i.e. 50m and 100m) and 5 satellites are used, the 60 GHz system and the 30 GHz system are better than the 15 GHz system. This is due to the relatively large variations in received signal intensity for the 60 GHz system and the 30 GHz system compared with the 15 GHz system (as shown in Fig. 7), thereby Eqn. (10) can tell more accurately if the flying object is close to the baseline.

VI. CONCLUSION

In this work, a new approach to positioning flying objects passively is proposed, by utilizing the microwave signals from LEO satellite constellations. Our analysis, both in terms of characterizing the relationship between the intensity of received signals and the attributes of flying objects, and the proposed signal processing method for passively positioning flying objects, is still very preliminary. To make the proposed approach work in practice, there are many more theoretical and simulations work to do. For example, is there a theoretical mechanism behind the "AM" signal observed in this paper? How to deal with multiple flying objects?

REFERENCES

[1] M. Youssef, M. Mah, and A. Agrawala, "Challenges: Device-free passive localization for wireless environments," in *Proc. 13th Annu. ACM Int. Conf. Mobile Comput. Netw.*, 2007, pp. 222–229.
[2] N. Patwari and J. Wilson, "RF sensor networks for device-free localization: Measurements, models, and algorithms," *Proc. IEEE*, vol. 98, no. 11, pp. 1961–1973, Nov. 2010.
[3] J. Liu, H. Liu, Y. Chen, Y. Wang, and C. Wang, "Wireless sensing for human activity: A survey," *IEEE Commun. Surveys Tuts.*, vol. 22, no. 3, pp. 1629–1645, 3rd Quart., 2020.
[4] *Starlink*. Accessed: Jan. 14, 2021. [Online]. Available: https://en.wikipedia.org/wiki/Starlink
[5] M. M. Azari, H. Sallouha, A. Chiumento, S. Rajendran, E. Vinogradov, and S. Pollin, "Key technologies and system trade-offs for detection and localization of amateur drones," *IEEE Commun. Mag.*, vol. 56, no. 1, pp. 51–57, Jan. 2018.
[6] I. Bisio, C. Garibotto, F. Lavagetto, A. Sciarrone, and S. Zappatore, "Blind detection: Advanced techniques for WiFi-based drone surveillance," *IEEE Trans. Veh. Technol.*, vol. 68, no. 1, pp. 938–946, Jan. 2019.
[7] I. Guvenc, F. Koohifar, S. Singh, M. L. Sichitiu, and D. Matolak, "Detection, tracking, and interdiction for amateur drones," *IEEE Commun. Mag.*, vol. 56, no. 4, pp. 75–81, Apr. 2018.
[8] A. Nussberger, H. Grabner, and L. Van Gool, "Robust aerial object tracking from an airborne platform," *IEEE Aerosp. Electron. Syst. Mag.*, vol. 31, no. 7, pp. 38–46, Jul. 2016.
[9] A. Rozantsev, V. Lepetit, and P. Fua, "Detecting flying objects using a single moving camera," *IEEE Trans. Pattern Anal. Mach. Intell.*, vol. 39, no. 5, pp. 879–892, May 2017.
[10] P. Sinha, Y. Yapici, I. Guvenc, E. Turgut, and M. Cenk Gursoy, "RSS-based detection of drones in the presence of RF interferers," 2019, *arXiv:1905.03471*. [Online]. Available: http://arxiv.org/abs/1905.03471
[11] *Malaysia Airlines Flight 370*. Accessed: Jan. 14, 2021. [Online]. Available: https://en.wikipedia.org/wiki/Malaysia_Airlines_Flight_370
[12] B. Sicardy, T. Widemann, E. Lellouch, and C. Veillet, "Large changes in Pluto's atmosphere as revealed by recent stellar occultations," *Nature*, vol. 424, no. 6945, pp. 168–170, Jul. 2003.
[13] N. Rodriguez-Alvarez, X. Bosch-Lluis, A. Camps, M. Vall-llossera, E. Valencia, J. F. Marchan-Hernandez, and I. Ramos-Perez, "Soil moisture retrieval using GNSS-R techniques: Experimental results over a bare soil field," *IEEE Trans. Geosci. Remote Sens.*, vol. 47, no. 11, pp. 3616–3624, Nov. 2009.
[14] M. Bevis, S. Businger, T. A. Herring, C. Rocken, R. A. Anthes, and R. H. Ware, "GPS meteorology: Remote sensing of atmospheric water vapor using the global positioning system," *J. Geophys. Res.*, vol. 97, no. D14, p. 15,787-15,801, Oct. 1992.
[15] E. R. Kursinski, "The active temperature, ozone and moisture microwave spectrometer (ATOMMS)," in *New Horizons Occultation Research*. Berlin, Germany: Springer, 2012, pp. 295–313.
[16] D. M. Ward, E. R. Kursinski, A. C. Otarola, M. Stovern, J. McGhee, A. Young, J. Hainsworth, J. Hagen, W. Sisk, and H. Reed, "Retrieval of water vapor using ground-based observations from a prototype ATOMMS active centimeter- and millimeter-wavelength occultation instrument," *Atmos. Meas. Techn.*, vol. 12, no. 3, pp. 1955–1977, Mar. 2019.
[17] L. Facheris and F. Cuccoli, "Global ECMWF analysis data for estimating the water vapor content between two LEO satellites through NDSA measurements," *IEEE Trans. Geosci. Remote Sens.*, vol. 56, no. 3, pp. 1546–1554, Mar. 2018.
[18] L. Facheris, F. Cuccoli, and F. Argenti, "Normalized differential spectral attenuation (NDSA) measurements between two LEO satellites: Performance analysis in the Ku/K-bands," *IEEE Trans. Geosci. Remote Sens.*, vol. 46, no. 8, pp. 2345–2356, Aug. 2008.
[19] G. Di Natale, S. Del Bianco, U. Cortesi, M. Gai, G. Macelloni, F. Montomoli, L. Rovai, S. Melani, A. Ortolani, A. Antonini, F. Cuccoli, L. Facheris, and A. Toccafondi, "Implementation and validation of a retrieval algorithm for profiling of water vapor from differential attenuation measurements at microwaves," *IEEE Trans. Geosci. Remote Sens.*, vol. 57, no. 8, pp. 5939–5948, Aug. 2019.
[20] H. Defeng, X. Lu, F. Xuxiang, and W. Wanyu, "A hypothesis of 3D rainfall tomography using satellite signals," *J. Commun. Inf. Netw.*, vol. 1, no. 1, pp. 134–142, Jun. 2016.
[21] L. Xu, X. Shen, D. D. Huang, X. Feng, and W. Wang, "Tomographic reconstruction of rainfall fields using satellite communication links," in *Proc. 23rd Asia–Pacific Conf. Commun. (APCC)*, Perth, WA, Australia, Dec. 2017, pp. 231–235.
[22] X. Shen, D. D. Huang, L. Xu, and X. Tang, "Reconstruction of vertical rainfall fields using satellite communication links," in *Proc. 23rd Asia–Pacific Conf. Commun. (APCC)*, Perth, WA, Australia, Dec. 2017, pp. 1–5.
[23] X. Shen, D. D. Huang, B. Song, C. Vincent, and R. Togneri, "3-D tomographic reconstruction of rain field using microwave signals from LEO satellites: Principle and simulation results," *IEEE Trans. Geosci. Remote Sens.*, vol. 57, no. 8, pp. 5434–5446, Aug. 2019.
[24] D. Huang, Y. Kuang, and J. Liu, "Angular spectrum analysis of the diffraction effect of microwave links by flying objects," *Opt. Techn.*, vol. 45, no. 1, pp. 1–5, Jan. 2019.
[25] D. B. Green and A. S. Obaidat, "An accurate line of sight propagation performance model for ad-hoc 802.11 wireless LAN (WLAN) devices," *Proc. ICC*, vol. 5, pp. 3424–3428, 2002.
[26] O. K. Ersoy, *Diffraction, Fourier Optics and Imaging*. Hoboken, NJ, USA: Wiley, 2006.

DEFENG DAVID HUANG (Senior Member, IEEE) received the B.E.E.E. and M.E.E.E. degrees from Tsinghua University, Beijing, China, in 1996 and 1999, respectively, both in electronic engineering, and the Ph.D. degree in electrical and electronic engineering from The Hong Kong University of Science and Technology (HKUST), Kowloon, Hong Kong, in 2004.

Before joining The University of Western Australia (UWA), he was a Lecturer with Tsinghua University. In 2005, he joined the School of Electrical, Electronic and Computer Engineering, UWA, as a Lecturer, where has been promoted to be a Professor, since 2011. He served as an Editor for the IEEE TRANSACTIONS ON WIRELESS COMMUNICATIONS and the IEEE WIRELESS COMMUNICATIONS LETTERS, from 2005 to 2011 and from 2011 to 2015, respectively, and an Editorial Assistant for the IEEE TRANSACTIONS ON WIRELESS COMMUNICATIONS, from 2002 to 2004.